This is a peer-reviewed, accepted author manuscript of the following research article: Zhang, L, Whyte, CG, Donaldson, CR, Ronald, K & Cross, AW 2024, 'Feedhorn synthesis using a parameterized aperture field distribution', IEEE Electron Device Letters , vol. 45, no. 2, pp. 252-255. https://doi.org/10.1109/LED.2023.3345222

Feedhorn synthesis using a parameterized aperture field distribution

Liang Zhang, Colin G. Whyte, Craig R. Donaldson, Kevin Ronald, and Adrian W. Cross

***Abstract*— In this paper, we present an improved method for synthesizing smooth-profiled horns. A direct connection between the mode compositions and far-field parameters was established by utilizing a parameterized aperture field distribution and the field decomposition method. It speeds up the optimization process by a factor of 5. The requirements for the aperture field to maintain a constant directivity were studied based on the method. A feedhorn was optimized for a W-band gyro-TWA with a 0.7 dB variation of the directivity within a bandwidth of 10%.**

***Index Terms*— horn, smoothly profiled horn, gyrotron travelling wave amplifier, Gaussian mode.**

I. Introduction

Gyro-devices based on cyclotron maser instability can generate high-power radiation at millimeter and sub-millimeter wave frequencies. The gyrotron travelling-wave amplifiers (gyro-TWAs) possess unique features such as controllable output power and phase, high power levels, and a balanced performance in terms of gain and bandwidth. They are attractive for diverse applications, including plasma diagnostics, radar systems, remote sensing, dynamic nuclear polarization (DNP), and electron spin resonance (ESR) spectroscopy [1-3].

A gyro-TWA using a helically corrugated waveguide as the interaction region, operating at W-band (75-110 GHz), has been developed at the University of Strathclyde [4, 5]. When driven by an axis-encircling electron beam (55 kV, 1.5 A) generated from a cusp electron gun [6], the saturated power exceeded 10 kW within a bandwidth of approximately 10%, spanning from 90 to 100 GHz. The output TE_{11} mode from the interaction region was converted into the fundamental Gaussian mode TEM_{00} and then coupled out of the gyro-TWA through a horn and a broadband multi-layer window [7-9].

The horn used in the gyro-TWA has more constraints compared to those used in atmospheric environments. These constraints include, (1) the reflection should be sufficiently low (<-30 dB) to prevent oscillations; (2) the horn should have high energy efficiency to reduce stray radiation inside the tubes and minimize thermal stress; (3) its structure should avoid having a large number of small grooves that can trap gas, leading to a long vacuum pumping time, to maintain compatibility with ultra-high vacuum levels; (4) it should be easy to machine, and no complicated brazing process should be required; (5) many materials, especially dielectric materials, cannot be used due to the potential risk of thermionic cathode poisoning and the relatively high temperature inside the gyro-TWA.

Various horns, including corrugated horns and a smoothly profiled horn, have been optimized and manufactured. The measurement results agreed well with the simulations [7, 8, 10]. The smoothly-profiled horn was found to be the optimal solution to balance the requirements, especially the low cost in manufacture and excellent vacuum compatibility.

This paper presents an improved method for synthesizing the smoothly-profiled horn. The combination of parameterized aperture field distribution and field decomposition method establishes a direct connection between the mode compositions and the far-field parameters, without the need for numerical field integrations. It provides a deeper into the patterns of the aperture field, to guide the design of horn antennas to achieve specific far-field performances, such as exploring the feasibility of achieving constant directivity over a certain bandwidth as studied in this paper.

II. Numerical Calculation Process of the Horns

A horn is a passive component, and the calculation of its performance follows these steps. Step one, the scattering matrix $S = \begin{bmatrix} S_{11} & S_{12} \\ S_{21} & S_{22} \end{bmatrix}$, which characterizes its transmission, mode conversion, and reflection, can be calculated using the generalized finite-difference time-domain (FDTD) method, the finite element method (FEM), or a specialized mode-matching method [11, 12]. With the scattering matrix and given the amplitudes and phases ($\boldsymbol{A_n}$) of input TE/TM modes $E_{TE/TM}$, the aperture field E_{ap}, represented as the sum of the output TE/TM modes with amplitudes and phases of $\boldsymbol{B_n}$, can be denoted as

$$E_{ap} = \sum \boldsymbol{B_n} \cdot E_{TE/TM} = \sum S_{21} \cdot \boldsymbol{A_n} \cdot E_{TE/TM} \quad (1)$$

Step two, the far-field radiation strength at an arbitrary spherical coordinate (R, θ, ϕ) can be calculated from E_{ap} using the aperture field method [13].

$$g(R,\theta,\phi) = \frac{ike^{-ikR}}{4\pi R}(1+\cos\theta)R_0^2 \int_0^1 \int_0^{2\pi} E_{ap}(\rho,\phi') \cdot e^{ik\rho R_0} \cdot \sin\theta \cdot \cos(\phi-\phi')\rho d\rho d\phi' \quad (2)$$

where $\rho = r/R_0$, k is the wavenumber in free space, and R_0 is the radius of the aperture. The directivity D, cross-polarization, and other far-field parameters can be calculated based on the function $g(R, \theta, \phi)$.

Step three will quantify the percentage of fundamental Gaussian mode E_{LG}. The coupling coefficient (ϵ) of the aperture field E_{ap} to E_{LG} can be calculated from

This work is under the support of Science and Technology Facilities Council (STFC) U.K by Cockcroft Phase 4 grant ST/V001612/1. L. Zhang (liang.zhang@strath.ac.uk), Colin Whyte, Kevin Ronald are with Department of Physics, SUPA, University of Strathclyde, Glasgow, G4 0NG, Scotland, UK, and Cockcroft Institute, Sci-Tech Daresbury, Cheshire, WA4 4AD, UK. Craig R. Donaldson and Adrian W. Cross are with Department of Physics, SUPA, University of Strathclyde, Glasgow, G4 0NG, Scotland, UK.

$$\epsilon = \frac{\left|\iint_{ap} E_{ap} \cdot E_{LG}^{*} ds\right|^{2}}{\iint_{ap} E_{ap} \cdot E_{ap}^{*} ds \cdot \iint_{\infty} E_{LG} \cdot E_{LG}^{*} ds} \quad (3)$$

By properly defining a set of goal functions, an optimizing routing can be used to search for the optimal structures of horns that satisfy the requirements. When examining the calculation steps, it can be seen that both (2) and (3) involve double integration. Typically, numerical integration is required since the analytical solution for double integration is normally unknown. A high accuracy of the integration requires a sufficiently large mesh number on the surface. Consequently, these steps become the most time-consuming tasks for the CPU during optimization, especially in the cases where repetitive calculations are necessary to evaluate horn performance at multiple frequency points for bandwidth analysis.

Significant improvement can be made if the expression of E_{ap} has an analytically integrable form in (2). The Gaussian function could be an option, given that it is well-known that the HE_{11} mode with a mixture of 85% TE_{11} and 15% TM_{11} modes, with a phase difference of π, will yield a ~98% Gaussian percentage. However, the Gaussian mode can not represent the aperture field in a general case. A generalized 3-parameter aperture field distribution has been proposed for antenna applications [14, 15], as follows:

$$E'_{ap}(\rho) = C + (1-C)\cdot(1-\rho^2)^{\alpha} \cdot \frac{\Lambda_{\alpha}(j\beta\sqrt{1-\rho^2})}{\Lambda_{\alpha}(j\beta)} \quad (4)$$

$$\Lambda_{\alpha}(\xi) = 2^{\alpha}\cdot\Gamma(\alpha)\cdot J_{\alpha}(\xi)/\xi^{\alpha} \quad (5)$$

where Γ and J_{α} are the Gamma function and Bessel function of the first kind, respectively. The parameters α, β, and C have the ranges of $\alpha \geq 0, \beta \geq 0$, and $C \in [0\ 1]$. The analytical expression for the far-field radiation, directivity, sidelobe levels, and beamwidth of E'_{ap} has been derived and presented in [14]. All three parameters have an impact on the far-field parameters. For instance, α has a significant influence on the sidelobe levels and how rapidly the field strength reduces from the waveguide center, which is equivalent to the beam waist if the aperture field is fitted as a fundamental Gaussian mode. β can be effectively used to tune the directivity, while C will have a big impact to the Gaussian percentage. $\alpha = 1, C = 0.25$, and $\beta \in [1, 5]$ will have a balanced performance to meet the major requirements for the applications.

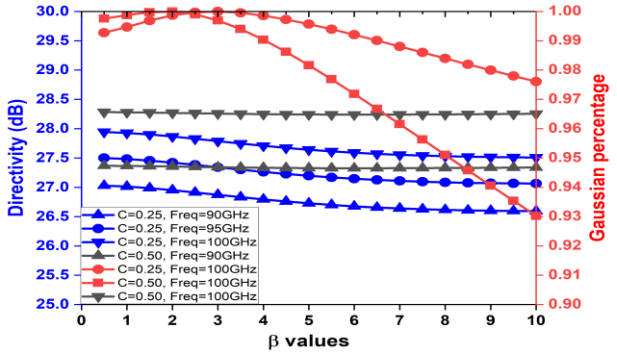

Fig. 1 The directivities and Gaussian percentages at different parameter values.

It is easy to find the optimal parameter range for α, β, and C to achieve the desired far-field parameters within the given frequency range. Fig. 1 shows the directivity and Gaussian percentages at various α, β, and C values. In the calculations, the aperture diameter is 25.12 mm and the frequency range is 90 to 100 GHz, which matches the multi-layer microwave window of the W-band gyro-TWA [16]. Fig. 1 shows that a high Gaussian percentage can be achieved by selecting the appropriate parameters in (4). With the same aperture field, the directivity is different at different frequencies.

One of the attractive features of the horn is to maintain a constant directivity over the required frequency band. Equation (2) indicates that with an identical aperture field pattern, the far-field properties will vary with frequency (resulting in changes in k values). However, it is challenging to quantify the level of these changes solely from the expression. The generalized 3-parameter aperture field distribution offers the opportunity to explore this efficiently, as shown in Fig. 1. The variation in directivity is approximately 1 dB within a bandwidth of 10% at an identical aperture field pattern.

The values of α, β and C need to change to achieve the same directivity over a bandwidth. The aperture field profile will change accordingly. Fig. 2(a) shows the β and C values to achieve a directivity of 27.2 dB. Fig. 2(b) plots the aperture field distributions at various frequencies. A fundamental Gaussian mode is plotted as well as the reference, demonstrating an excellent overlap with the aperture field distribution at 98 GHz. At lower frequencies, the waist of the field profile (when fitted into a Gaussian profile) should be smaller, indicating higher power concentration at the center of the horn. Fig. 2 also shows that at other frequencies, such as 90 GHz, the Gaussian percentage will decrease. Maintaining a constant directivity requires a trade-off in performance.

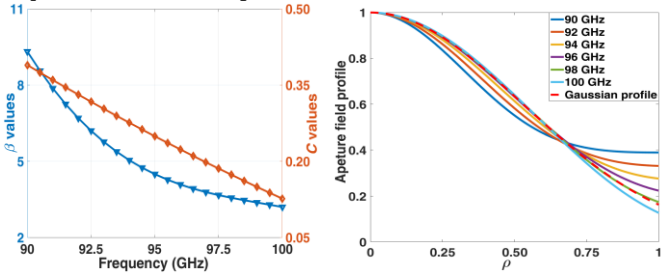

(a) (b)

Fig. 2 The variation of β and C for the same directivity (a), and the corresponding aperture field distributions at different frequencies (b).

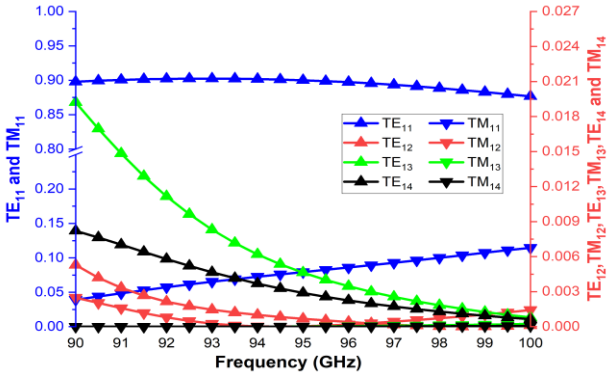

Fig. 3 The amplitude of TE/TM modes.

The synthesis of the horn can, be simplified to find a horn

structure that produces the desired aperture field profile E'_{ap}. Decomposing E'_{ap} into the orthogonal TE/TM mode sets as $E'_{ap} = \sum \boldsymbol{B'_n} \cdot E_{TE/TM}$ can further simplify the question. Where

$$B'_n = \frac{\iint_{ap} E'_{ap} \cdot E^*_{TE/TM} ds}{\left(\iint_{ap} E'_{ap} \cdot E^*_{ap} ds \cdot \iint_{ap} E_{TE/TM} \cdot E^*_{TE/TM} ds\right)^{1/2}} \quad (6)$$

Fig. 3 shows the calculation results of (6) using the aperture field distribution provided in Fig. 2. Only the first few modes (TE_{11}, TM_{11}, TE_{12}, TM_{12}, TE_{13}, TM_{13}, TE_{14}, and TM_{14}) are considered. The higher-order modes have significantly lower amplitudes, and their contributions can be neglected. It should be noted that the TE_{13} mode exhibits relatively high amplitude at lower frequencies, indicating that considering only TE_{11} and TM_{11} are inadequate for horns with a high Gaussian content. The TE modes have the same phases, whereas the TM modes have a phase difference of π to the TE modes. The horn design will then be transformed into finding a structure that can achieve $\boldsymbol{B_n} \approx \boldsymbol{B'_n}$ [17]. Consequently, only the first step of horn calculation is required. Only one calculation for (6) is needed to obtain the desired TE/TM mode combination before optimization, significantly reducing the computation resource and time.

III. W-BAND SMOOTH-PROFILED HORN

The proposed method is suitable for different types of horns. For the application of gyro-TWA, the smooth-profiled horn [18] is an optimal choice to balance various requirements. Its axially symmetric structure allows for fast calculations using the mode-matching method, and its simple profile makes it much more cost-effective to manufacture compared to the corrugated horn.

The smooth-profiled horn in [8] was redesigned using the improved method. The horn profile was based on the sine function. In the region of $0 \le z \le L_1$, the inner radius is

$$R(z) = R_0 + \frac{(R_1 - R_0)z}{L_1}\left[\sin\left(\frac{\pi}{2} \cdot \frac{z}{L_1}\right)\right]^{p_1 + (p_2 - p_1)\frac{z}{L_1}}, 0 \le z \le L_1$$
$$R(z) = R_1 + (R_2 - R_1)(z - L_1)/(L - L_1),\ L_1 \le z \le L \quad (7)$$

where $R_0 = 2.80$ mm, and $R_2 = 12.56$ mm. R_1, L_1, p_1, p_2 and L are free parameters. Their ranges of value were $R_1 \in [R_0, R_2], L_1 \in [45\text{ mm}, 120\text{ mm}]$, $L \in [80\text{ mm}, 280\text{ mm}]$, $p_1 \in [1.5, 3.5]$, and $p_2 \in [0.6, 3.5]$. The goal functions were

$$\text{Fun1} = \sum_f^N W(f) \cdot |B'_n(f) - B_n(f)|^2$$
$$\text{Fun2} = \frac{1}{N}\sum_f^N S_{11}(f) \quad (8)$$

Fun1 is the sum of the differences of the mode compositions at the aperture over the sample frequency f. Different weight functions (W) can be applied to prioritize various frequency components. Fun2 is the average reflection (S_{11}) of the horn.

The optimization was carried out on a PC with an Intel i7 3.4 GHz CPU (8 cores, 16 threads), and 64 GB RAM. The computation time required to simulate 400 sets of parameters was 1 hour, which is 5 times faster than the original method because there was no need for the intensive computations of (2) and (3). Fig. 4 presents a comparison of the original and two optimized horn profiles and the simulation results. Similar to the original design, the optimised profile (1) maintained a simple shape with a nonlinear profile over ~70 mm, and a linear phasing section. It has a similar performance compared with the original design, including ~98% Gaussian percentage, less than -25 dB cross-polarisation and reflections less than -55 dB. The optimization (1) horn has a directivity 0.4 dB higher than the original design over the frequency band while the variation was similar at ~1.2 dB.

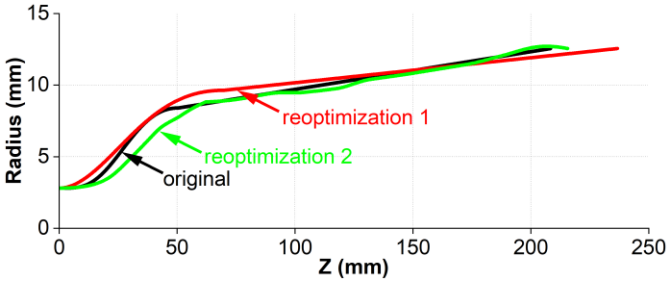

(a)

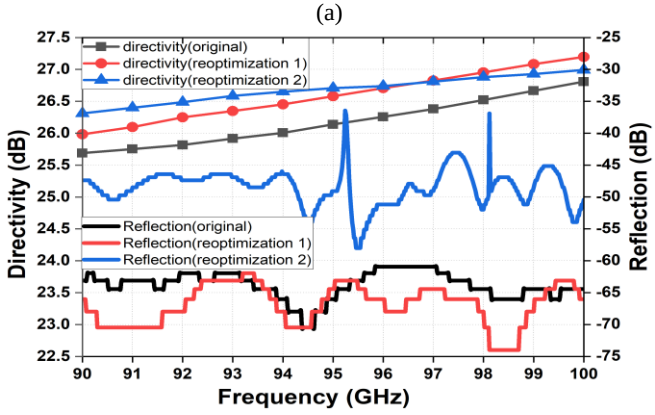

(b)

Fig. 4 The horn profiles (a), and the directivities and reflection of the horns (b).

Another optimization (2) was carried out on a more complex horn profile, which was created by superimposing (7) with a spline curve controlled by 10 additional free parameters. This allowed to explore a broader range of horn profiles to achieve a reduced variation in the directivity. Although the optimized results show that directivity variation can be reduced to 0.7 dB, as indicated in Fig. 2, reducing directivity variation requires large variation in the horn profile to achieve substantial mode conversion across the bandwidth. This increases the manufacting difficulty and it increased the reflection to -35 dB. High reflection is not attractive for the gyro-TWA application.

IV. DISCUSSION AND CONCLUSION

In this paper, an improved method for synthesizing horn design is presented. By introducing a parameterized aperture field distribution and the field decomposition method, the connection between the TE/TM mode composition and the far-field parameters was established, which significantly speeds up the horn optimization process. It also enables the exploration of the required aperture field pattern to achieve particular far-field parameters, such as the feasibility of maintaining a constant directivity over a certain bandwidth. Furthermore, the present method can be applied directly to other types of output launchers, and is not limited to the smoothly-profiled horn studied in this paper.

REFERENCES

[1] J. Benford and J. Swegle, "Applications of high power microwaves," in *1992 9th International Conference on High-Power Particle Beams*, 25-29 May 1992 1992, vol. 1, pp. 341-348, doi: 10.1109/PLASMA.1992.697928.

[2] E. A. Nanni, A. B. Barnes, R. G. Griffin, and R. J. Temkin, "THz Dynamic Nuclear Polarization NMR," *IEEE Transactions on Terahertz Science and Technology*, vol. 1, no. 1, pp. 145-163, 2011, doi: 10.1109/TTHZ.2011.2159546.

[3] S. Coda, S. Alberti, P. Blanchard, T. P. Goodman, M. A. Henderson, P. Nikkola, Y. Peysson and O. Sauter, "Electron cyclotron current drive and suprathermal electron dynamics in the TCV tokamak," *Nucl. Fusion*, vol. 43, no. 11, p. 1361, 2003/11/03 2003, doi: 10.1088/0029-5515/43/11/008.

[4] W. He, C. R. Donaldson, L. Zhang, K. Ronald, P. McElhinney, and A. W. Cross, "High Power Wideband Gyrotron Backward Wave Oscillator Operating towards the Terahertz Region," *Phys. Rev. Lett.*, vol. 110, no. 16, p. 165101, 2013, doi: 10.1103/PhysRevLett.110.165101.

[5] W. He, C. R. Donaldson, L. Zhang, K. Ronald, A. D. R. Phelps, and A. W. Cross, "Broadband Amplification of Low-Terahertz Signals Using Axis-Encircling Electrons in a Helically Corrugated Interaction Region," *Phys. Rev. Lett.*, vol. 119, no. 18, p. 184801, Oct. 2017, doi: 10.1103/PhysRevLett.119.184801.

[6] C. R. Donaldson, W. He, A. W. Cross, F. Li, A. D. R. Phelps, L. Zhang, K. Ronald, C. W. Robertson, C. G. Whyte, and A. R. Young, "A cusp electron gun for millimeter wave gyrodevices," *Appl. Phys. Lett.*, vol. 96, no. 14, p. 141501, 2010, doi: 10.1063/1.3374888.

[7] P. McElhinney, C. R. Donaldson, J. E. McKay, L. Zhang, D. A. Robertson, R. I. Hunter, G. M. Smith, W. He, and A. W. Cross, "An Output Coupler for a W-Band High Power Wideband Gyroamplifier," *IEEE Trans. Electron Devices*, vol. 64, no. 4, pp. 1763-1766, 2017, doi: 10.1109/TED.2017.2660304.

[8] L. Zhang, W. He, C. R. Donaldson, G. M. Smith, D. A. Robertson, R. I. Hunter, and A. W. Cross, "Optimization and Measurement of a Smoothly Profiled Horn for a W-Band Gyro-TWA," *IEEE Trans. Electron Devices*, vol. 64, no. 6, pp. 2665-2669, Jun 2017, doi: 10.1109/ted.2017.2687949.

[9] C. R. Donaldson, P. McElhinney, L. Zhang, and W. He, "Wide-Band HE11 Mode Terahertz Wave Windows for Gyro-Amplifiers," *IEEE Transactions on Terahertz Science and Technology*, vol. 6, no. 1, pp. 108-112, June 2016, doi: 10.1109/TTHZ.2015.2495221.

[10] P. McElhinney, C. R. Donaldson, L. Zhang, and W. He, "A high directivity broadband corrugated horn for W-band gyro-devices," *IEEE Trans. Antennas Propag.*, vol. 61, no. 3, pp. 1453-1456, 2013, doi: 10.1109/TAP.2012.2228840.

[11] T. Itoh, *Numerical Techniques for Microwave and Millimeter-Wave Passive Structures*. Wiley, 1989.

[12] G. L. James, "Analysis and Design of TE11-to-HE11 Corrugated Cylindrical Waveguide Mode Converters," *IEEE Trans. Microwave Theory Techn.*, vol. 29, no. 10, pp. 1059-1066, 1981, doi: 10.1109/TMTT.1981.1130499.

[13] A. Ludwig, "Radiation pattern synthesis for circular aperture horn antennas," *IEEE Trans. Antennas Propag.*, vol. 14, no. 4, pp. 434-440, 1966, doi: 10.1109/TAP.1966.1138723.

[14] D. W. Duan and Y. Rahmat-Samii, "A generalized three-parameter (3-P) aperture distribution for antenna applications," *IEEE Trans. Antennas Propag.*, vol. 40, no. 6, pp. 697-713, 1992, doi: 10.1109/8.144605.

[15] J. Fondevila-Gomez, I. C. Coleman, J. A. Rodriguez-Gonzalez, and F. Ares-Pena, "A Cautionary Note on Optimization [Antenna Designer's Notebook]," *IEEE Antennas and Propagation Magazine*, vol. 55, no. 5, pp. 136-139, 2013, doi: 10.1109/MAP.2013.6735486.

[16] C. R. Donaldson, W. He, L. Zhang, and A. W. Cross, "A W-Band Multi-Layer Microwave Window for Pulsed Operation of Gyro-Devices," *IEEE Microw. Wireless Compon. Lett.*, vol. 23, no. 5, pp. 237-239, May 2013, doi: 10.1109/LMWC.2013.2251619.

[17] O. M. Bucci, T. Isernia, and A. F. Morabito, "Optimal Synthesis of Directivity Constrained Pencil Beams by Means of Circularly Symmetric Aperture Fields," *IEEE Antennas and Wireless Propagation Letters*, vol. 8, pp. 1386-1389, 2009, doi: 10.1109/LAWP.2009.2039189.

[18] C. Granet, G. L. James, R. Bolton, and G. Moorey, "A smooth-walled spline-profile horn as an alternative to the corrugated horn for wide band millimeter-wave applications," *IEEE Trans. Antennas Propag.*, vol. 52, no. 3, pp. 848-854, 2004, doi: 10.1109/TAP.2004.825156.